PHYSICAL REVIEW A VOLUME 44, NUMBER 3 1 AUGUST 1991

Spectroscopy and multichannel quantum-defect theory analysis of the *np* Rydberg series of H_3

M. C. Bordas,* L. J. Lembo,† and H. Helm
Molecular Physics Department, SRI International, Menlo Park, California 94025
(Received 2 April 1991)

The lowest *np* Rydberg series of triatomic hydrogen has been studied using optical-optical double-resonance excitation from the metastable $2p^2A_2''$ level. Bound states, detected by field ionization as well as autoionizing states of the *p* series are characterized using rotational multichannel quantum-defect theory. Deviations from the calculations appear when vibrational interactions give rise to predissociation below threshold or autoionizing interlopers above threshold. The *np* Rydberg manifold of H_3 provides an almost complete panorama of channel interactions in a polyatomic molecule: rotational and vibrational interactions and autoionization with rich Fano profile structure as well as predissociation.

I. INTRODUCTION

The Rydberg states of triatomic hydrogen resemble in many respects quasihydrogenic atomic Rydberg states. The small size of the core molecular ion H_3^+ and its associated small multipole moments allow for only weak rotational interactions in the nonpenetrating Rydberg series with angular momentum $l \geq 2$. The energy levels of the *nd* and *nf* Rydberg series appear [1–3] in excitation as very regular quasihydrogenic channels, converging to a single state of the core ion. We show here that the *p*-electron Rydberg series are quite different, in that the electron approaches the core close enough that short-range electron-core interactions play an important role [4]. The richness of the observed features in the bound spectrum as well as in the continuum makes the H_3 *np* series a very general example of channel interactions in a polyatomic molecule.

Photoionization [1–3,5,6] and photodissociation [7–10] studies of the fundamentally unstable H_3 molecule have been an active field of research since the first analysis of the emission bands of H_3 by Herzberg and coworkers [11–15] in the early 1980s. Photoexcitation studies of H_3 conducted thus far have relied largely upon the metastability [16] of the lowest rotational level of the $\tilde{B}\ 2p^2A_2''$ state. This level has a lifetime of 640 ns [17]. The dominant $2p$ character of the outer electron in the metastable state gives rise to *R*-branch type transitions into *s*-type and *d*-type Rydberg states, which have been detected by means of electric-field ionization [1,2], photoionization [5,6], and predissociation [8,9]. Using double-resonance techniques and a low-lying *s* or *d* state as intermediate, one can also study odd-*l* states, as for example the *nf* series [3] or the *np* series presented in this paper. Here, in a two-color stepwise excitation scheme, we first access the nonvibrating $3s^2A_1'$ state and then probe with a second tunable laser, the *p*-electron series in the bound-state region, and in the region above the lowest ionization threshold.

Rotational interactions among the *p*-electron Rydberg states have been already discussed from a theoretical point of view [18] and we will show in the following the relevance of the frame transformation theory of the *l*-uncoupling effect in H_3. What renders the study of the *np* Rydberg states of H_3 particularly enlightening is that their spectrum displays examples of noninteracting Rydberg series ($N=0$ or 1), and of two series interacting in the discrete region and in the Beutler-Fano continuum ($N=2$). In addition, vibrational interactions appear in the discrete spectrum, where they cause predissociation, as well as in the continuum, where the presence of vibrational interlopers is evidenced by strong resonances and windows in the excitation spectrum.

The *np* Rydberg series contain states that match the symmetry of the electronic ground state of H_3, the sole dissociative continuum below the ionization threshold. An understanding of the *np* Rydberg states therefore appears as key towards an explanation of the occurrence of the very localized predissociations that have been observed in the H_3 molecule [19] and that are attributed to accidental vibrational perturbations that establish coupling paths [20] from high-*n* Rydberg states into the repulsive ground state of H_3.

We begin with a short description of the energy levels and symmetries of H_3 relevant to the present experiment, followed by the presentation of the experimental technique used. Before discussing the experimental results, we give a brief review of the equations of the multichannel quantum-defect theory (MQDT) that we use in our analysis of line positions and excitation intensities. Following this we present the experimental spectra of the *np* series in three fundamentally disting regions: (1) the discrete spectrum below the first ortho level of the ground state of the H_3^+ ion ($N^+=1$, $K^+=0$); (2) the Beutler-Fano region between the two lowest ortho levels of H_3^+ ($N^+=1$ and 3, $K^+=0$), where we see a classic example of rotational autoionization; and (3) the continuum region above the $N^+=3$ level of the ion. The experimental results are then analyzed in the framework of MQDT and we finally discuss the possibility of including vibrational interactions to account for the presence of intense interloper lines and competition between dissociation and autoionization.

II. EXPERIMENT

A. Experimental principle

An energy-level diagram of triatomic hydrogen in D_{3h} geometry is shown in Fig. 1 together with the excitation scheme used in the present experiments. The figure gives the location of the lowest states involved in our optical scheme and the unstable ground state of H_3 in relation to the two- and three-body neutral and ionic dissociation limits.

The lowest long-lived H_3 state is the lowest rotational level of the $2p^2A_2''$ state. This level has a symmetric nuclear spin wave function (ortho-H_3), and it is characterized by the quantum numbers $N=0$, $K=0$. Here and in the following, N and K (respectively N^+ and K^+) represent the total angular momentum, excluding spin, and its projection onto the top axis for the neutral molecule (respectively the ion). This metastable state is nearly purely described by a configuration built from a $2p(a_2'')$ electronic orbital on the lowest ortholevel of the H_3^+ ion: $N^+=1$, $K^+=0$.

The excitation of the np Rydberg series is achieved in a two-step process (see Fig. 1). A first photon $h\nu_1$ (16 694.97 cm^{-1}) [12] induces transition from the vibrationless metastable level of the $\tilde{B}$ state ($N=0$) to the $3s^2A_1'(N=1,\ v_1=v_2=0)$ intermediate state (v_1 and v_2 denote, respectively, the symmetric stretch and the degenerate mode vibrational quantum numbers of the molecule):

$$2p^2A_2''(N''=0)+h\nu_1\rightarrow 3s^2A_1'(N'=1)\ . \qquad (1)$$

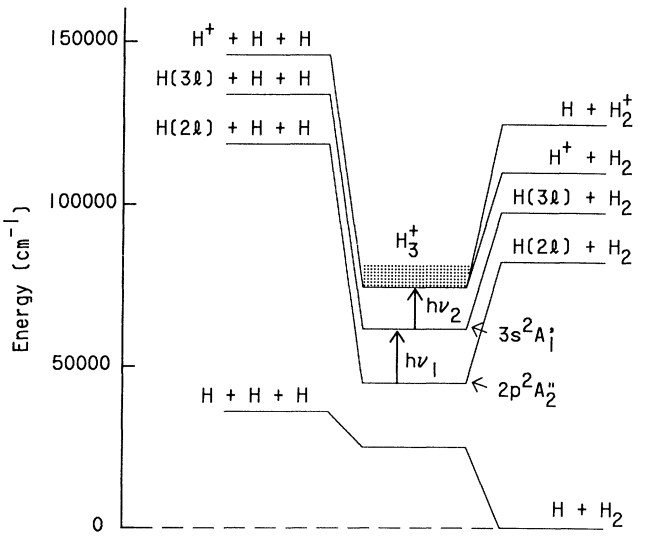

FIG. 1. Energy diagram for H_3 states relevant for the excitation scheme to high-lying p Rydberg states. The first laser ($h\nu_1$) is fixed to the $2p^2A_2''\rightarrow 3s^2A_1'$ transition. The second laser ($h\nu_2$) is scanned in the vicinity of the two lowest ionization limits of ortho-H_3.

Following the selective excitation of the vibrationless $3s$ state, a second laser is tuned through the ionization threshold regions to excite the p-electron Rydberg series:

$$3s^2A_1'(N'=1)+h\nu_2\rightarrow np(N=0,\ 1,\text{or } 2)\ . \qquad (2)$$

For the second excitation step, transitions to levels with $N=0$, 1, and 2 are allowed by electric dipole selection rules. We show in Fig. 2 how states with these N values can be generated by combining a p-type electron with the core ion $N^+=3$, giving a series with $N=2$, and with the core ion $N^+=1$, giving series with $N=0$, 1, and 2. Depending on the relative orientation of the polarization axes of the two photons $h\nu_1$ and $h\nu_2$, one can excite only the $M_N=0$ (parallel polarizations) or only the $M_N=1$ levels (perpendicular polarizations). In the first case, only $N=0$ or 2 states can be excited, while in the latter case, transitions to $N=0$ states are forbidden and only $N=1$ or 2 states are excited. This second excitation step is detected by ionization of the Rydberg states. Levels below the threshold appear due to field ionization; levels above threshold generally autoionize or they are induced to ionize by an external electric field. The first laser, which excited the $3s$ state, is kept at an intensity low enough to avoid a background photoionization signal from 1+1 photon ionization. The second laser operates at moderate intensity to avoid saturation broadening in the np series members.

During the second excitation step, diagonal transitions (i.e., without change in the vibrational excitation of the core) are expected to dominate over nondiagonal transitions (Δv_1 or $\Delta v_2\neq 0$). The potential-energy surface of the $3s^2A_1'$ state is very similar to the surface of the ion, and therefore to those of the p Rydberg states with high values of n. Hence, upward transitions from the $3s$ state, accompanied by a change of vibrational excitation, are not expected, with the exception of transitions to vibrational interlopers with low principal quantum number for which the poor Franck-Condon factor is offset by the greater electronic transition moment.

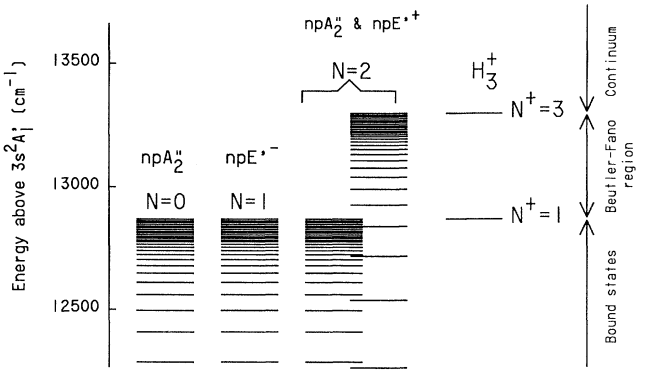

FIG. 2. Schematic representation of the core states of the lowest p Rydberg series.

In the framework of Hund's case (b), the *np* Rydberg series involved in our experiments are either np^2A_2'' or np^2E', which are analogous to $np\sigma$ and $np\pi$ states of a diatomic molecule. The $N=0$ and 1 series are pure np^2A_2'' and np^2E', respectively, while members of the $N=2$ series are a mixture of the two symmetries. Selection rules and line intensities as well as symmetry classification and the related passage from Hund's case (b) to Hund's case (d) will be discussed in the theoretical section of this paper.

B. Experimental setup

The experimental setup has been described previously [1,3]. H_3^+ ions are extracted from a hollow-cathode hydrogen discharge at an energy of 1.5 keV. The H_3 molecules are produced by charge exchange of H_3^+ in a cesium vapor cell. The resulting neutral beam, purged of residual ions by a small electric deflection field, contains only molecules in the rotationaless level of the long-lived $\tilde{B}\ 2p^2A_2''$ state [17]. In an ultrahigh-vacuum chamber, the neutral beam interacts with two superimposed coaxial dye laser beams along a 120-cm-long interaction region. Care is taken to avoid residual electric fields in the excitation region [19]. Both lasers have a pulse duration of about 15 ns, a bandwidth of 0.15 cm^{-1}, and a spot size of about 5 mm^2. The first laser $h\nu_1$ is tuned to the $3s \leftarrow 2p$ transition (16 694.97 cm^{-1}) which is easily saturated with pulse energies as low as 50 μJ. The second laser (1 mJ/pulse) excites the molecules from the 3*s* state to the *np* series. Due to the shoft lifetime [17,21] of the 3*s* intermediate state (10 ns $> \tau \geq$ 0.8 ns), the second laser is not delayed with respect to the first. It is scanned from $\sim$100 cm^{-1} below the first orthoionization limit ($N^+=1$) to $\sim$1300 cm^{-1} above the limit, corresponding to a wavelength scan from 700 and 790 nm. A fixed ionizing field of about 1.7 kV/cm at the entrance of an energy and mass analyzer is used for field ionization of the bound states lying below the threshold or for deflection of the ions created in the autoionization processes. The resulting ions of mass 3 are detected on a microchannel plate and counted. The mass selection ensures that we do not detect H^+ or H_2^+ ions produced in dissociative processes.

III. THEORY

The appearance of the excitation spectra of the *np* Rydberg states is strongly influenced by rotational channel interactions. The theory suitable for the description of these interactions, MQDT, is well developed [21-25] and we outline below how it is applied in the case of H_3. This framework will be used in the following section to identify position, intensity, and line shape of the transitions to the *np* states. Numerous instances of vibrational channel interactions also appear in our spectra. While these could formally be incorporated in the theory, the current information on the participating core states and their vibrational interaction via the Rydberg electron is too limited for the theory to be predictive.

The basis of the theory is that a Rydberg electron moves essentially outside the core, in a region where it experiences a pure Coulombic potential. The effects of short-range interactions are described by a limited number of parameters that are basically independent of the energy: the quantum defects, which are empirically determined from the experimental spectra, and a molecular frame transformation matrix that we can calculate exactly.

A. MQDT wave function

A key point is to introduce two different basis sets describing the electron-core interaction at infinity (collision channels) or near the origin (close-coupling channels) and to match the expansion of the molecular wave function in these two bases in the intermediate space. These sets must satisfy boundary conditions respectively at infinity and near the core.

The collision-channel wave functions Ψ_i are defined by

$$\Psi_i = \chi_i(f_i \cos\pi\nu_i + g_i \sin\pi\nu_i) , \tag{3}$$

where χ_i contains the core wave function and the angular and/or spin part of the electronic wave function. The radial wave function is expressed as a linear combination of regular $[f_i(\nu_i,l,r)]$ and irregular $[g_i(\nu_i,l,r)]$ Coulomb wave functions (defined to be energy normalized for positive energies) and matches the boundary conditions as the electron coordinate r tends to infinity. The coefficients $\cos(\pi\nu_i)$ and $\sin(\pi\nu_i)$ ensure that the wave function ψ_i behaves correctly at large separation of the electron from the core.

The close-coupling channel wave functions Ψ_α take into account the non-Coulombic short-range interactions via the introduction of the quantum defects μ_α ($\pi\mu_\alpha$ represents the phase shift due to the short-range interactions) and the unitary transformation matrix U which relates collision channels i to close-coupling channels α:

$$\Psi_\alpha = \sum_i \chi_i U_{i\alpha}(f_i \cos\pi\mu_\alpha - g_i \sin\pi\mu_\alpha) . \tag{4}$$

The total wave function Ψ of the system is written as a linear combination of the Ψ_i or of the Ψ_α functions, respectively:

$$\Psi = \sum_i B_i \Psi_i = \sum_\alpha A_\alpha \Psi_\alpha . \tag{5}$$

The total energy of the system is defined by

$$E = \varepsilon_i + I_i , \tag{6}$$

where e_i, the electron energy is connected to the quantum number n_i via

$$\varepsilon_i = -\mathcal{R}/\nu_i^2 . \tag{7}$$

B. The *U* matrix

The transformation matrix U is the unitary matrix connecting close-coupling and ionization (or collision) channels. The ionization channels are described by the quantum numbers of the ionic core N^+, K^+, and Γ^+ (electronic species), the angular momentum of the Rydberg

electron l, the total angular momentum of the molecule (neglecting spin) N and its projection onto the symmetry axis M_N. In the close-coupled channels, Γ^+, K^+, l, N, and M_N are still good quantum numbers, with the addition of the electronic species of the neutral molecule, Γ. Therefore the U matrix reduces to a transformation from the basis where N^+ is defined [Hund's case (d) basis] to the basis where Γ is well defined [Hund's case (a) or (b) basis]. In contrast to atomic physics, where the $LS-jj$ coupling transformation only gives an approximation for the U matrix, the molecular U matrix is strictly the transformation from Hund's case (d) to Hund's case (b) because at short distance Γ is an exact quantum number and at large distance N^+ is an exact quantum number. As noted before, only the odd-N^+ levels of H_3^+ are present in the ionization channel basis because we start from a $K^+=0$, ortho level of H_3^+. The general expression for the U matrix in the case of a polyatomic molecule in D_{3h} geometry may be derived from the general expression for a diatomic molecule given by Chang and Fano.[23] Exchanging their electronic lable $\overline{\Lambda}$ for our quantum number K^+ adapts their formula (Eq. (A9) of Ref. [23]) to triatomic hydrogen. For the different N values that we can access, we have the following U matrices (see Fig. 2)

(i) For $N=0$, only one channel exists ($U=1$). This channel is termed np^2A_2'' in the close-coupled basis and $np(N^+=1)$ in the collision basis.

(ii) For $N=1$, also only one channel exists ($U=1$). This channel is termed np^2E' in the close-coupling basis and $np(N^+=1)$ in the collision basis.

(iii) For $N=2$, two channels appear. They are np^2A_2'' and np^2E' in the close-coupling basis and $np(N^+=1)$ or $np(N^+=3)$ in the collision basis. The transformation matrix in this case is

$$U=\begin{array}{c} \\ \langle N^+=1| \\ \langle N^+=3| \end{array}\begin{array}{c} \begin{array}{cc} |^2A_2''\rangle & |^2E'\rangle \end{array} \\ \begin{pmatrix} \sqrt{2/5} & \sqrt{3/5} \\ -\sqrt{3/5} & \sqrt{2/5} \end{pmatrix} \end{array} . \tag{8}$$

C. Boundary conditions

Boundary conditions and compatibility of Eqs. (3), (6), and (7) impose, for each ionization channel i,

$$\sum_\alpha U_{i\alpha}\sin[\pi(\nu_i+\mu_\alpha)]A_\alpha=0 , \tag{9a}$$

$$\sum_\alpha U_{i\alpha}\cos[\pi(\nu_i+\mu_\alpha)]A_\alpha=B_i , \tag{9b}$$

or the equivalent formulation for each close-coupling channel α:

$$\sum_i U_{i\alpha}\sin[\pi(\nu_i+\mu_\alpha)]B_i=0 , \tag{10a}$$

$$\sum_i U_{i\alpha}\cos[\pi(\nu_i+\mu_\alpha)]B_i=A_\alpha . \tag{10b}$$

A nontrivial solution of (9a) or (10a) requires that

$$\det\{U_{i\alpha}\sin[\pi(\nu_i+\mu_\alpha]\}=0 , \tag{11}$$

while Eqs. (9b) and (10b) allow us to change the representation from Hund's case (b) to Hund's case (d) and reciprocally. These equations hold regardless of whether or not some channels are open to ionization, with the condition that when a channel i is open ($\varepsilon_i>0$), the effective quantum number ν_i must be replaced by a scattering phase shift τ.

1. Discrete spectrum

In the discrete spectrum, the effective quantum number νi_i is real and the electron's energies are negative. Equation (11), together with relations (6) and (7), give the level energies, determining the entire discrete spectrum. For bound states, the normalization factor $\mathcal{N}$ for the wave function Ψ is such that [22]

$$\mathcal{N}^2=\sum_i \nu_i^3\Big(\sum_\alpha A_{i\alpha}\cos[\pi(\nu_i+\mu_\alpha)]\Big)^2 . \tag{12}$$

To calculate the intensity of the transition between the initial state and the Rydberg state Ψ we need the transition matrix elements in the close-coupling basis, T_α, or in the ionization basis, T_i, connected by

$$T_i=\sum_\alpha \frac{1}{\cos(\pi\mu\alpha)}U_{i\alpha}T_\alpha . \tag{13}$$

The intensity of the transition is simply

$$I=\frac{(\sum_\alpha T_\alpha A_\alpha)^2}{\mathcal{N}^2}=\frac{(\sum_i T_i B_i)^2}{\mathcal{N}^2} . \tag{14}$$

The transition matrix elements are functions of the total angular momentum N and of the relative polarization of the two lasers which determines M_N. We now calculate the elements T_α where we chose the polarization axis of $h\nu_1$ as the quantization axis. The general form of the transition matrix elements between an initial state well described in the Hund's case (d) $\{\rho_i,N^+,N_i,l_i,M_i\}$ and a final state described in the Hund's case (b) basis by $\{\rho_f,N_f,\Gamma_f l_f,M_f\}$ can be calculated using standard angular momentum algebra[26] (ρ represents the other quantum number: n, spin, etc.). In the case where both lasers are polarized along the same axis ($M_N=0$) we have

$$T_{\parallel}=U_{N^+\Gamma}\begin{pmatrix} N_f & 1 & N_i \\ 0 & 0 & 0 \end{pmatrix}\sqrt{(2N_i+1)(2N_f+1)}\delta_{N_i^+N_f}\begin{Bmatrix} l_f & N_f & N_f \\ N_i & l_i & 1 \end{Bmatrix}\langle\rho_f l_f\|Q_{el}\|\rho_i l_i\rangle . \tag{15a}$$

If the two lasers are polarized along two perpendicular axes ($M_N=1$)

$$T^{\perp}_{\Gamma}=U_{N^+\Gamma}\begin{bmatrix} N_f & 1 & N_i \\ 1 & -1 & 0 \end{bmatrix}\sqrt{(2N_i+1)(2N_f+1)}\delta_{N_i^+N_f}\begin{Bmatrix} l_f & N_{f^+} & N_f \\ N_i & l_i & 1 \end{Bmatrix}\langle \rho_f l_f \| Q_{\rm el} \| \rho_i l_i \rangle \ , \tag{15b}$$

where $U_{N^+\Gamma}$ is the transformation matrix between Hund's case (d) ($i \equiv N^+$) and Hund's case (b) ($\alpha \equiv \Gamma$).

In the particular case of a transition between the $3s^2A_1'$ state ($l_i=0$, $N^+=1$, $N=1$) and an np Rydberg state we have for parallel linear polarizations, the following. For $P(1)$,

$$T^{\parallel}_{A_2''}=\tfrac{1}{3}T_{\rm el}, \quad T^{\parallel}_{E'}=0 \ .$$

For $Q(1)$,

$$T^{\parallel}_{A_2''}=0, \quad T^{\parallel}_{E'}=0 \ .$$

For $R(1)$,

$$T_{A_2''}=\sqrt{4/45}T_{el}, \quad T^{\parallel}_{E'}=\sqrt{2/15}T_{\rm el} \ .$$

And for perpendicular polarizations, for $P(1)$,

$$T^{\perp}_{A_2''}=0, \quad T^{\parallel}_{E'}=0 \ .$$

For $Q(1)$,

$$T^{\perp}_{A_2''}=0, \quad T^{\perp}_{E'}=\tfrac{1}{6}T_{\rm el} \ .$$

For $R(1)$,

$$T^{\perp}_{A_2''}=\sqrt{1/15}T_{\rm el}, \quad T^{\perp}_{E'}=\sqrt{1/10}T_{\rm el} \ , \tag{16}$$

where $T_{\rm el}$ is the electronic part of the transition moment:

$$T_{\rm el}=\langle np \| Q_{\rm el} \| 3s^2A_1' \rangle \ . \tag{17}$$

2. Beutler-Fano region

Above the first ionization limit, the $N=0$ and 1 series are in the ionization continuum while the $N=2$ series between the $N^+=1$ and 3 levels of the ion is subject to rotational autoionization. In this case, the effective quantum number $\nu_{N^+=3}$ is real while $\nu_{N^+=1}$ is purely imaginary. Then $\nu_{N^+=1}$ must be replaced by a phase shift $-\tau$ related to $\nu_{N^+=3}$ by Eq. (11), while Eq. (4) has no meaning for ν_1 in this region. With a single channel open, as is the case here, the problem is trivial and Eq. (11) has only one solution for a given energy:

$$\Psi=\frac{\sum_i B_i\Psi_i}{\mathcal{N}} \ . \tag{18}$$

The summation over i extends over the channels $i=(N^+=1)$ and $i=(N^+=3)$, with Ψ_i defined by Eq. (3) and the normalization factor $\mathcal{N}$ given by the very simple expression

$$\mathcal{N}^2=\sum_{i^*} B_i^2=B^2_{(N^+=1)} \ , \tag{19}$$

where i^* means that channel i is open.

The photoionization intensity in the Beutler-Fano region is then calculated using Eqs. (14), (16), and (17).

3. Continuum

The density of oscillator strength evolves smoothly from the bound-state region to the Beutler-Fano region and to the true continuum. For the $N=0$ and 1 series the continuum is located above the $N^+=1$ level of the ion while, for the $N=2$ series, it is located above the $N^+=3$ level of the ion. In the continuum, there exist as many independent solutions as there are open channels. These solutions may be arbitrarily chosen to be the close-coupled wave functions Ψ_α defined by Eq. (4). No structure appears in the continuum unless vibrational or electronic interactions with excited core states occur.

IV. EXPERIMENTAL RESULTS

Figure 3 shows a spectrum for a photon energy $h\nu_2$ scanned between about 12 770 and 14 200 $\rm cm^{-1}$. This spectrum is recorded with parallel laser polarization (i.e., $M_N=0$) and is normalized to the laser intensity. We note here that the lower energy limit of detecting the excitation spectrum is imposed by the field-ionization efficiency. For the experimental setup used here, the efficiency decreases rapidly when the principal quantum number n is lower than 30. Here and in the following, the photon energy is relative to the $3s^2A_1'$ state. The "absolute" energy relative to the lowest metastable state of H_3 may be obtained by adding [12] 16 694.97 $\rm cm^{-1}$ to this value.

Excitation of the Rydberg states occurs from a single level of the $3s$ state, with $N=1$ ($K=0$) and no vibration.

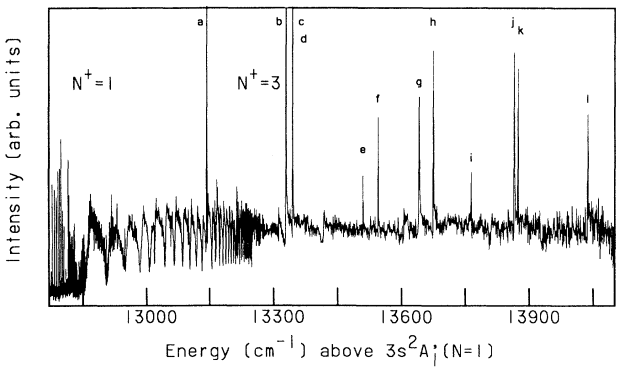

FIG. 3. Excitation spectrum of H_3 $3s^2A_1'$ from 12 700 to 14 200 $\rm cm^{-1}$ ($M_N=0$) showing the three distincts regions: the discrete spectrum below $N^+=1$, the Beutler-Fano region between the limits $N^+=1$ and 3, and the continuum beyond $N^+=3$.

Since vibrationally diagonal transitions (i.e., $\Delta v_1 = \Delta v_2 = 0$ are by far stronger than nondiagonal, the dominant observed series are the vibrationless $N=0$ 1, and 2 *np* series converging to the $N^+=1$ or 3 ($K^+=0$) levels of the ion. These two ionization limits separate the spectrum into three different regions. These regions are indicated schematically in Fig. 2 and 3 and they correspond to the three cases described in the preceding section. Below the lowest ortho level of H_3^+ $N^+=1$, $K^+=0$ (photon energy lower than 12 867.6 cm^{-1}), the Rydberg states are strictly stable relative to autoionization because no accessible ionization continuum exists. An ensemble of discrete narrow peaks is observed in this region. This portion of the spectrum is shown on an expanded scale in Fig. 4. Between the $N^+=1$ and $N^+=3$ levels of the ion ($12\,867.6 < h\nu_2 < 13\,297.5$ cm^{-1}), the $N^+=1$ continuum is open and the *np* Rydberg states can autoionize. This region, referred to as the Beutler-Fano region, exhibits a structured continuum where the $N^+=3$ series members appear as dips in the ion signal. The reason for the window formation is that we start from a 3*s* state that has a pure $N^+=1$ core. Note that the window formation only applies to the $N=2$ *np* Rydberg series. The $N=0$ and 1 Rydberg states are built from an *np* electron surrounding an $N^+=1$ core. Their excitation spectrum in the region above threshold is a pure continuum. These continua underly the $N=2$ features and they are the reason why the intensity minima do not reach zero value. An expanded view of the Beutler-Fano region is given in Fig. 5. Finally, above the$N^+=3$ level ($h\nu_2 > 13\,297.5$ cm^{-1}) we are in the true continuum of all vibrationless series with $N=0$, 1, and 2.

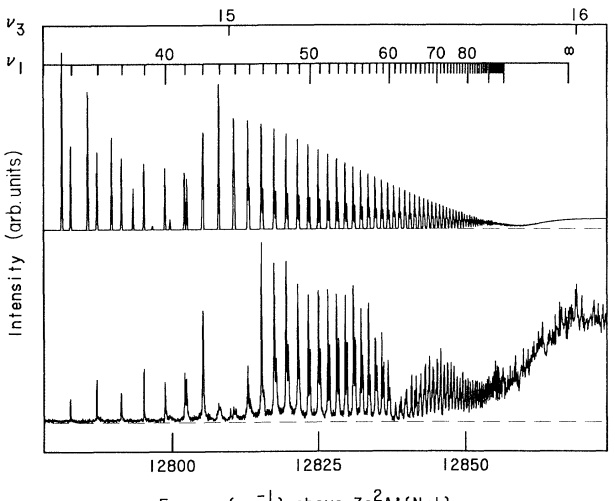

FIG. 4. Experimental spectrum ($M_N=0$, bottom) and MQDT simulation (top) below the first ionization limit (discrete-state region). The numbers at the top are the effective quantum numbers ν_1 relative to the first ionization limit $N^+=1$ and the integer quantum numbers ν_3, relative to the limit $N^+=3$. The calculated line positions are in good agreement with the experiment while the line intensities are obviously perturbed.

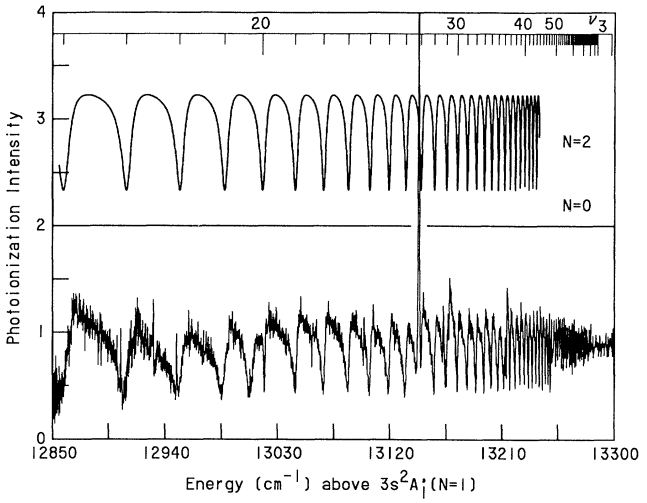

FIG. 5. Beutler-Fano spectrum with $M_N=0$ (bottom) and MQDT simulation (top). General agreement between theory and experiment is observed except for the presence of localized perturbations such as the extra window resonance near $\nu_3=20$ and a strong interloper near $\nu_3=27$.

This region should in principle be a flat continuum with the exception of strong autoionizing lines pertaining to vibrationally excited series. We now discuss in more detail each of these three regions.

A. The discrete spectrum: $h\nu_2 < 12\,867.6$ cm^{-1}

A close-up of the bound-state region is displayed in Fig. 4 together with a two-channel quantum-defect calculation. As mentioned previously, with our excitation scheme, one can selectively excite the $N=0$ and 2 ($M_N=0$) series if the two lasers are linearly polarized along the same axis or the $N=1$ and 2 ($M_N=\pm 1$) series if they are polarized along the perpendicular axis. An immediate advantage of this characteristic is the possibility of studying directly the unperturbed $npA''(N=0)$ and $npE'(N=1)$ series. We can derive their quantum defects using a simple Rydberg formula:

$$E_\alpha = E(H_3^+ N^+=1, K^+=0) - \frac{\mathcal{R}}{(n-\mu_\alpha)^2}\ , \qquad (20)$$

where α designates the symmetry of the series (pA'' or pE') and μ_α its quantum defect. The Rydberg constant $\mathcal{R}$ is 109 717.40 cm^{-1} for H_3. The knowledge of these two quantum defects is then sufficient to analyze the $N=2$ series where A'' and E' symmetry are mixed by rotational interaction (l uncoupling). The spectrum of Fig. 4 has been recorded with $M_N=0$ and hence only $N=0$ and 2 lines are visible. The energy position of each line is very precisely calculated with a two-channel MQDT treatment as shown by the good agreement between experiment and calculated line position in Fig. 4. The values of the quantum defect fitted to the experimental

line positions are

$$\mu_{pA_2''} = 0.05 \pm 0.01 \ , \tag{21a}$$

$$\mu_{pE'} = 0.39 \pm 0.01 \ . \tag{21b}$$

The agreement between experimental and calculated values is generally better than our experimental resolution (0.15 cm^{-1}) with a standard error of about 0.03 cm^{-1} for the unperturbed $N=0$ lines and 0.10 cm^{-1} for the $N=2$ lines. Note that the calculated spectrum has been broadened to a width of 0.15 cm^{-1} comparable to our experimental resolution. However, noticeable disagreements are observed as far as the line intensities are concerned. Three points are worthy of mention here.

(1) The calculation predicts that the intensity of the $N=2$ series converging to the $N^+=1$ limit should vanish near $n=40$. This is due to the presence of the $n=15$ interloper state of the $N^+=3$ series near this energy. The theory also predicts that lines corresponding to $N=2$ states with $n<38$ should be more intense than the companion $N=0$ lines. In fact, no $N=2$ states are observed below $n \approx 41$ while the $N=0$ lines are present in the experimental spectrum.

(2) Additional intensity windows appear in the experimental spectrum around $n=43$ and 61. Near $n=61$ only the $N=2$ series is diminished in intensity but for $n=43$ both series are affected.

(3) Finally, the experimental intensities of the low-n lines are weaker than expected in comparison to the intensity of the high-n lines. The overall scaling rule of $1/n^3$ is not observed in the experimental spectrum. A hydrogenic simulation shows that with the ionizing-field value and with the geometry (time of flight of the neutrals in the detection field) we use, field ionization must be 100% efficient above $n=35$; therefore the field-ionization efficiency should not be responsible for this deviation.

In the present experiment, the H_3 molecules excited to a discrete state below the ionization limit have a time of flight between 1 and 4 μs in a field-free space before reaching the field-ionization detector. Thus, if any decay process is fast enough to occur during that time frame, no ions will be detected and the observed line intensity may be low even for strong transitions. Low-lying states of H_3 are known to be rapidly predissociated [17,21] on picosecond to nanosecond time scales due to interactions with the vibrational continuum of the dissociative ground state. It is therefore not really surprising to observe such decay processes, occurring on a longer time scale, for the higher Rydberg states. However, the localization of this process to very confined regions and at even very high n values (the n^3 scaling factor holds also for predissociative lifetimes in Rydberg states) remains to be clarified.

The region around $n=61$ is of particular interest and we have already discussed this region in a previous paper [19] where we show that predissociation of the *nd* states near $n=61$ is induced by extremely weak fields by coupling of *nd* states with the *np* series. Figure 6 is an enlargement of the *p*-series spectrum in this region. This portion of the spectrum shows that the intensity of the $N=2$, *np* Rydberg series displays a broad window extending from about $n=60$ to 64, centered at $n=61$ where the

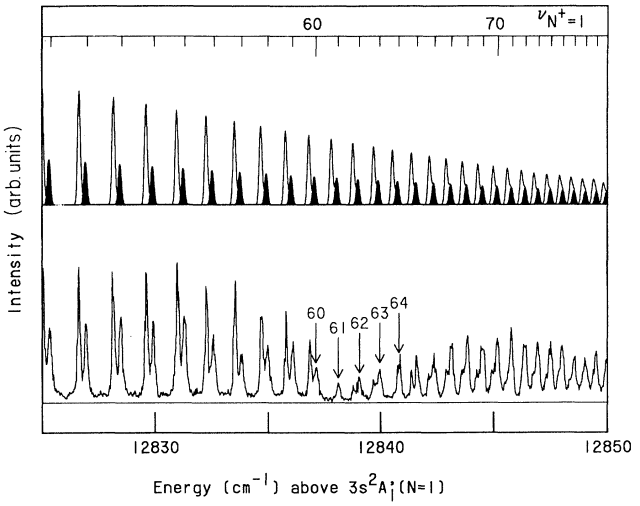

FIG. 6. Close-up of the discrete spectrum in the vicinity of $n=61$ (bottom) and MQDT simulation (top). In the calculated spectrum the $N=0$ lines are filled in black. The numbers 60 to 64 indicate the $np(N=0)$ Rydberg states. The $n=61$ and 64 ($N=2$) lines are clearly missing. Below $\nu_1=60$, calculated and experimental intensity match, while at higher energy the experimental intensity of the $N=2$ lines is smaller than predicted.

intensity of the $N=2$ transition is zero. By contrast, the $N=0$, *np* series is not visibly affected. In the calculated spectrum of Fig. 6, the $N=0$ lines are marked in black for clarity. The calculated intensity ratio between $N=0$ and 2 lines is in agreement with our observations for levels lying below the window resonance but it appears inverted for the higher Rydberg members. The wide energy range over which the intensity perturbation occurs points to the existence of a giant resonance, the origin of which is considered to be a homogeneous (electrostatic) interaction [27] of the Rydberg states with an interloper state $|A\rangle$.

$$61p(N=2) \leftrightarrow |A\rangle(N=2) \ . \tag{22a}$$

The interloper state in turn is predissociated to the ground state of H_3:

$$|A\rangle(N=2) \rightarrow 2p^2E'(N=2) \ . \tag{22b}$$

From the electric-field-induced predissociation of the *nd* Rydberg states near $n=61$, we have deduced [19] that the state $|A\rangle$ is a low-n pE' state ($n=2$ or 3) with sufficient vibrational excitation to be quasidegenerate with the $61p$ vibrationless state. The predissociation rate of the interloper $|A\rangle$ is found [19] to fall into the range $4\times10^8 < \Gamma_A < 4\times10^{10}$ s^{-1}. A more precise characterization of the core state responsible for the $n=61$ window is not possible at this point. A similar coupling mechanism to a predissociated state with lower principal quantum number and excited core vibration is likely responsible for the window formation near $n=43$ (see Fig. 4). But also its assignment and the origin for the absence of $N=2$ states below $n=38$ remain open at this point.

The knowledge of the two quantum defects $\mu_{pA''}$ and

$\mu_{pE'}$ obtained by fitting the discrete spectrum is sufficient, together with the knowledge of the energy levels of the ion, to analyze precisely the Beutler-Fano region, which we discuss next.

B. The Beutler-Fano region: $12\,867.6 < h\nu_2 < 13\,297.5$ cm^{-1}

This region, located between the $N^+=1$ and 3 ortho levels of H_3^+, is displayed in Fig. 5. It is the region where rotational autoionization occurs. According to the excitation scheme used, this spectrum is a superposition of the $N=2$ series, the structured continuum, where $N^+=3$ members appear as dips in the $N^+=1$ continuum with the flat continuum of the $N=0$ or 1 series. The theory predicts that the appearance of the $M_N=0$ or 1 Beutler-Fano region is qualitatively similar except for the larger relative intensity of the flat continuum of $N=1$ when perpendicular polarizations are chosen. The upper spectrum in Fig. 5 gives the prediction of the two-channel MQDT calculation for $M_N=0$. The quantum defects derived from the analysis of the discrete spectrum are used in this simulation without adjustment. The agreement between experiment and theory is satisfactory, especially for the energy dependence of the photoionization intensity. This is opposite to the situation for discrete spectrum (see Fig. 4). The very regular series of typically asymmetric Fano profiles in the calculated spectrum matches almost perfectly the experimental spectrum. However, localized shifts of the position of the dips appear as well as several interloper resonances and windows.

The better agreement between calculated and experimental intensities in the Beutler-Fano region in comparison with the discrete spectrum is easy to understand. Most of the disagreement in the discrete spectrum comes from the fact that, during the few microseconds the Rydberg molecules exist before being field ionized, relatively slow decay processes (of the order of 1 μs) such as radiative decay or predissociation have time to occur. On the contrary, in the Beutler-Fano region, rotational autoionization is very fast, as seen from the broad width of the dips, and radiative processes are not able to compete with autoionization. Thus, unless rapid predissociation is induced by an interloper state, all the excited molecules may be detected. More quantitatively, we can estimate the lifetime of the Beutler-Fano resonances using the classic formula [28]

$$\tau \approx \frac{\nu^3_{N^+=3}}{2\pi^2 \mathcal{R} c\,(\mu_{pE'}-\mu_{pA''})^2} \approx 1.33\times 10^{-16}\nu^3_{N^+=3}\ \text{s} . \qquad (23)$$

According to this expression, the lifetime of the first resonance ($\nu_{N^+=3}=17$) above the $N^+=1$ threshold is as short as 0.7 ps, while for $\nu_{N^+=3}=50$ the lifetime is still less than 20 ps. It is clear that rotational autoionization is the largely dominant process.

We now address the discrepancies that appear between calculation and experiment in the Beutler-Fano region. The spectrum in Fig. 7 exhibits several additional dips in the autoionization signal that are not expected from the MQDT treatment. A substantial shift in the position of the $N^+=3$ series members occurs near $\nu_{N^+=3}=20$, and

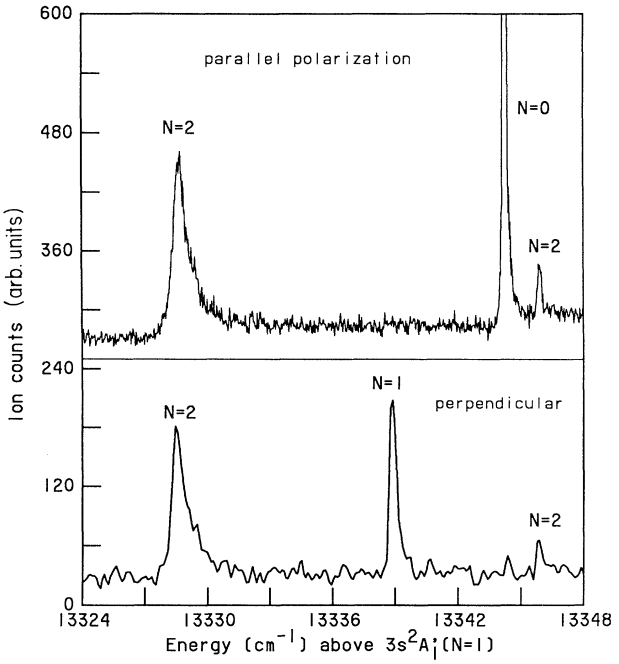

FIG. 7. Close-up of some vibrational interlopers appearing in the continuum of the vibrationless series: $M_N=0$ (top) and $M_N=1$ (bottom). These spectra demonstrate the assignment of the angular momentum quantum number N.

at least one very strong line appears near $\nu_{N^+=3}=27$. The only possible origin of these lines and dips, rather narrow as compared to the rotationally autoionizing lines, is that they correspond to Rydberg states built on a vibrationally excited core. Electronically excited core states [29] of H_3^+ lie too high in energy to be involved in the perturbations observed here. The large number of such features above the second ionization limit may eventually help us to specify the nature of these interlopers. In the case of the dip near $\nu_{N^+=3}=20$, the interaction between the vibrationless np series and the interloper must be very strong because the $n=20$ member of the $N^+=3$ series is shifted by about 10 cm^{-1} to the red while the levels below are shifted to a smaller degree. The interloper itself appears as a dip in the $N=2$ continuum. We therefore require that the interloper itself is characterized by the quantum number $N=2$. The dip occurs either due to a destructive interference that lowers the excitation probability, or else because this interloper has a predissociation lifetime shofter than its rovibrational autoionization lifetime. On the other hand, the extremely strong transition at 13 143 cm^{-1} ($\nu_{N^+=3}\approx 27$) does not seem to induce any noticeable shift in the vibrationless lines in its vicinity. This is an indication that the coupling between this interloper and the $N^+=3(0,0)$ series is relatively small and its angular momentum could be either $N=0$ or 2.

C. The true continuum: $h\nu_2 > 13\,297.5\ \text{cm}^{-1}$

If vibrational interactions and off-diagonal transitions were negligible, the continuum above $N^+=3$ should appear with a constant photoionization intensity proportional to T_1^2. In fact, the examination of the broad $M_N=0$ spectrum (Fig. 3) shows that even this region displays significant structure. The dozen intense lines observed in this spectrum, together with the line lying in the Beutler-Fano region and a few measured for $M_N=1$ are reported in Table I together with a tentative assignment for some of these transitions. The assignment of the angular momentum quantum number N is possible when spectra were recorded with perpendicular and parallel orientation of the laser polarization. If a line appears in both spectra it is likely to be an $N=2$ line and if a line appears only when parallel (perpendicular) polarizations are used it is a transition to $N=0$ ($N=1$). An example is given in Fig. 7. The assignment of a principal quantum number or of vibrational quantum numbers is more difficult and, so far, all assignments must be taken as tentative.

The difficulty in assigning the interloper states is related to the large number of core states that may participate in resonance formation. We show in Fig. 8 the lowest vibrational levels [30] of the ion core. The vibrational levels are separated into states with electronic symmetry A_1 and E. The most intense transitions to interlopers with core states of A_1 symmetry will be to npE' and npA_2'' states as is the case for excitation to Rydberg states with the vibrationless core. On the other hand, core states with E symmetry require degenerate mode excitation in the electronic transition and therefore the Rydberg electron must either remain $l=0$ or possibly change into $l=2$. The assignments suggested in Table I use the core energies calculated by Tennyson and Henderson [30] and they are chosen on the basis of consistency of the effective quantum defects with those known from the vibrationless states at low principal quantum number. Significant vibrational excitation is observed for several intense resonances. In view of our recent observations of vibrational excitation in transitions from the vibrationless $2p^2A_2''$ level to $3s$, $3p$, and $3d$ states [5,9] this is not surprising if we keep in mind that the electronic transition moment to the interloper states is weighted relative to the high-n Rydberg states by the cubed ratio of principal quantum numbers involved. We note (footnote a in Table I) that many resonances remain unassigned. We suspect that some of these will involve electronic states with principal quantum numbers $n=3$ and 2 with very high core excitation.

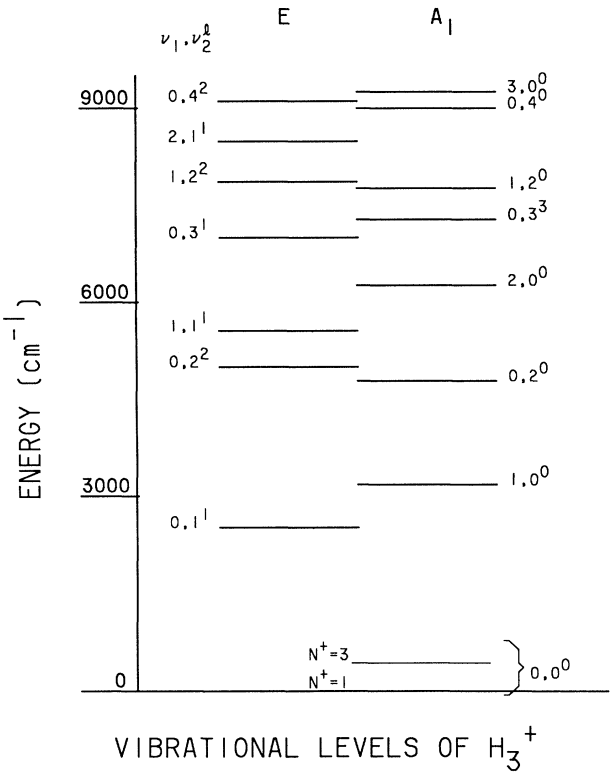

FIG. 8. Low-lying vibrational core states of H_3^+ of A_1 and E symmetry as calculated by Tennyson and Henderson [30]. The single level with A_2 symmetry in this energy range ($\nu_1=0,\nu_2=3,l=3$) at 7493 cm^{-1}, is omitted. The rotational spacing of the lowest ortholevels of H_3^+ with quantum number $K^+=0$ is shown for comparison with the vibrational gaps.

A surprising feature in the excitation spectrum are four fairly strong members of the $nf3$ Rydberg series (see Table I). The assignment of these transitions,

$$3s^2A_1'(N'=1)+h\nu\rightarrow nf3\ , \tag{24}$$

is based on the observation of an effective quantum defect of zero ($\delta<0.01$) for the final states involved. The members observed belong to the nf series that converges to the core level $N^+=3$, $K^+=0$ of the vibrationless ground state. We may think of two ways how intensity can be generated for the transitions (24). These transitions require an effective change in core rotation from $N^+=1$ to 3. For one the $3s^2A_1'(N'=1)$ lower state lies 1036 cm^{-1} below the $3d^2A_1'(N'=1)$ level which has a core wave function that is greater than 99% of $N^+=3$ character [3]. Hence, through s-d mixing the $3s$ state may pick up a minute attribute of the $N^+=3$ core that is required to drive a transition to the $nf3$ series. Alternatively, the transition strength derives from p-f mixing in the final states between the $(N=2)nf3$ members and the $(N=2)np3$ series which is accessed in the "allowed" transition (2).

V. CONCLUSION

Given the well-established success of MQDT in analyzing molecular spectra, it is hardly surprising that the very simple rotational theory used in the present work reproduces fairly well many of the observed features. Exceptions occur due to vibrational interactions, which are not included in the theoretical model. It is in principle possi-

TABLE I. Vibrational and rotational interlopers[a] appearing in the photoexcitation spectrum of the vibrationless $3s^2A_1'(N=1)$ state. Excitation linewidths δ are given where measured. Tentative assignments for the Rydberg states and the core states of H_3^+ are also given. The effective quantum numbers of the Rydberg states are calculated using the core energies of Tennyson and Henderson [30].

Label	$h\nu_1$ (cm^{-1})	δ (cm^{-1})	N	$nl\Gamma$	$(N^+,G^+\nu_1\nu_2^l)$	ν_{eff}
	12 809.6			$15fE'$	$(3,0,0,0^0)$	15.00
	12 868.8			$16fE'$	$(3,0,0,0^0)$	16.00
	12 875.9	W[b]		$5pE'$	$(3,0,0,2^0)$	4.59
	12 918.0			$17fE'$	$(3,0,0,0^0)$	17.00
	12 958.9			$18fE'$	$(3,0,0,0^0)$	18.00
	13 125.5	1.0	1	$4pA_2''$	$(1,0,0,3^3)$	3.92
(a)	13 143.0	0.8	2	$5pA_2''$	$(1,0,0,2^0)$	4.94
(b)	13 328.7	1.0	2	$4pE'$	$(1,0,0,4^0)$	3.59
	13 338.9	0.4	1	$5sA_1'$	$(1,0,0,2^2)$	4.92
(c)	13 344.3	0.2	0	$7dA_1'$	$(2,0,0,1^1)$	6.98
(d)	13 345.9	0.2	2	$7dA_1'$	$(2,0,0,1^1)$	6.99
(e)	13 510.1	0.4		$7pE'$	$(1,0,1,0^0)$	6.58
(f)	13 545.8	0.3		$4pE'$	$(1,0,0,4^0)$	3.63
(g)	13 641.7	1.8		$4pA_2''$	$(1,0,0,2^0)$	3.96
(h)	13 674.7	0.6		$4pE'$	$(1,0,3,0^0)$	3.61
(i)	13 764.1	0.3		$7pA_2''$	$(1,0,1,0^0)$	6.94
(j)	13 864.8	0.8		$4pE'$	$(3,0,0,4^0)$	3.61
(k)	13 873.7	0.3		$4pE'$	$(1,0,3,0^0)$	3.65
(l)	14 037.0	0.4		$7dA_1'$	$(1,0,0,1^1)$	8.98

[a]Additional, weaker resonances appear at the following photon energies: 12 905.0, 12 930.9, 12 949.2, 12 966.4, 13 107.0, 13 162.6, 13 380.5, 13 506.6, 13 547.0, 14 029.7 cm^{-1}. Additional window resonances appear at 13 019.5, 13 057.8, 13 099.4, 13 312.5, and at 13 418.0 cm^{-1}.
[b]Window in excitation intensity.

ble to extent the MQDT to include the vibrational channels [28,31] and to treat the competition between predissociation and autoionization [32]. On the basis of the very precise calculations of the H_3^+ levels by Tennyson and co-workers [30,33] and the predictions on the variation of the quantum defect with nuclear geometry by Nader and Jungen [20] such an analysis may soon be tractable.

ACKNOWLEDGMENTS

Stimulating discussions with Dr. D. L. Huestis greatly helped progress in this investigation. This research was supported by the United States Air Force Aero Propulsion Laboratory, Wright Patterson Air Force Base, under Contract No. F 33615-90-C-2007. One of us (M.C.B.) wishes to acknowledge a NATO travel grant.

*Permanent address: Laboratoire de Spectrométrie Ionique et Moléculaire, Université Claude-Bernard Lyon I, Bâtiment 205, 43 Boulevard-du 11 Novembre, 69622 Villeurbanne CEDEX, France.
†Permanent address: TRW, Space & Technology Group, MS R1/1176, One Space Park Drive, Redondo Beach, CA 90278.

[1] H. Helm, Phys. Rev. Lett. **56**, 42 (1986); Phys. Rev. A **38**, 3425 (1988).
[2] A. Dohdy, W. Ketterle, H. P. Messmer, and H. Walther, Chem. Phys. Lett. **151**, 133 (1988).
[3] L. J. Lembo, C. Bordas, and H. Helm, Phys. Rev. A **42**, 6660 (1990).
[4] H. F. King and K. Morokuma, J. Chem. Phys. **71**, 3213 (1979).
[5] L. J. Lembo, H. Helm, and D. L. Huestis, J. Chem. Phys. **90**, 5299 (1989).
[6] L. J. Lembo, A. Petit, and H. Helm, Phys. Rev. A **39**, 3721 (1989).
[7] S. F. Selgren and G. I. Gellene, Chem. Phys. Lett. **146**, 485 (1988).
[8] P. C. Cosby and H. Helm, Phys. Rev. Lett. **61**, 298 (1988).
[9] L. J. Lembo and H. Helm, Chem. Phys. Lett. **163**, 425 (1989).
[10] P. C. Cosby and H. Helm, Chem. Phys. Lett. **152**, 71 (1988).
[11] I. Dabrowski and G. Herzberg, Can. J. Phys. **58**, 1238 (1980).
[12] G. Herzberg and J. K. G. Watson, Can. J. Phys. **58**, 1250 (1980).
[13] G. Herzberg, H. Lew, J. J. Sloan, and J. K. G. Watson, Can. J. Phys. **59**, 428 (1981).
[14] G. Herzberg, J. T. Hougen, and J. K. G. Watson, Can. J. Phys. **60**, 1261 (1982).
[15] J. K. G. Watson, S. C. Foster, A. R. W. McKellar, P. Bernath, T. Amano, F. S. Pan, W. M. Crofton, R. S. Altman, and T. Oka, Can J. Phys. **62**, 1875 (1984).
[16] G. I. Gellene and R. F. Porter, J. Chem. Phys. **79**, 5975 (1983).
[17] C. Bordas, P. C. Cosby, and H. Helm, J. Chem. Phys. **93**,

6303 (1990).
[18] Shao-hua Pan and K. T. Lu, Phys. Rev. A **37**, 299 (1988).
[19] C. Bordas and H. Helm, Phys. Rev. A **43**, 3645 (1991).
[20] Ch. Nader and M. Jungen, Chem. Phys. **70**, 189 (1982).
[21] N. Bjerre, I. Hazell, and D. C. Lorents (unpublished).
[22] U. Fano, Phys. Rev. A **2**, 353 (1970).
[23] E. S. Chang and U. Fano, Phys. Rev. A **6**, 173 (1972).
[24] C. H. Greene and Ch. Jungen, Adv. At. Mol. Phys. **21**, 51 (1985).
[25] C. H. Greene, U. Fano, and G. Strinati, Phys. Rev. A **19**, 1485 (1979).
[26] A. R. Edmonds, *Angular Momentum in Quantum Mechanics* (Princeton University Press, Princeton, NJ, 1960).
[27] H. Lefebvre-Brion and R. Field, *Perturbations in the Spectra of Diatomic Molecules* (Academic, New York, 1986).
[28] Ch. Jungen and D. Dill, J. Chem. Phys. **73**, 3338 (1980); Ch. Jungen and M. Raoult, *ibid.* **74**, 3388 (1981).
[29] D. Talbi and R. P. Saxon, J. Chem. Phys. **89**, 2235 (1988).
[30] J. Tennyson and J. R. Henderson, J. Chem. Phys. **91**, 3815 (1989).
[31] C. Bordas, P. Labastie, J. Chevaleyre, and M. Broyer, Chem. Phys. **129**, 21 (1989).
[32] A. Giusti-Suzor and Ch. Jungen, J. Chem. Phys. **80**, 986 (1984).
[33] J. Tennyson, O. Brass, and E. Pollak, J. Chem. Phys. **92**, 3005 (1990).